Pacific Northwest
NATIONAL LABORATORY

PNNL-34994

Solid Phase Processing at the Extreme

September 2023

Glenn J. Grant
Anthony P. Reynolds
Xiao Li
Md. Reza-E-Rabby
Ayoub Soulami
Lei Li

U.S. DEPARTMENT OF ENERGY

Prepared for the U.S. Department of Energy
under Contract DE-AC05-76RL01830

DISCLAIMER

PACIFIC NORTHWEST NATIONAL LABORATORY
operated by
BATTELLE
for the
UNITED STATES DEPARTMENT OF ENERGY
under Contract DE-AC05-76RL01830

Printed in the United States of America

Available to DOE and DOE contractors from
the Office of Scientific and Technical Information,
P.O. Box 62, Oak Ridge, TN 37831-0062
www.osti.gov
ph: (865) 576-8401
fox: (865) 576-5728
email: reports@osti.gov

Available to the public from the National Technical Information Service
5301 Shawnee Rd., Alexandria, VA 22312
ph: (800) 553-NTIS (6847)
or (703) 605-6000
email: info@ntis.gov
Online ordering: http://www.ntis.gov

PNNL-34994

Solid Phase Processing at the Extreme

September 2023

Glenn J. Grant
Anthony P. Reynolds
Xiao Li
Md. Reza-E-Rabby
Ayoub Soulami
Lei Li

Prepared for
the U.S. Department of Energy
under Contract DE-AC05-76RL01830

Pacific Northwest National Laboratory
Richland, Washington 99354

Abstract

The effective application of high-flow-stress materials in the realm of Solid Phase Processing frequently necessitates operating at elevated temperatures and substantially high force. These rigorous processing conditions give rise to intricate predicaments concerning the durability of the tools and dies involved, as well as the efficient utilization of process energy. This project is centered on the investigation of the fundamental scientific aspects inherent to these challenges. We aim to delve into the details of how materials react when subjected to intense shear forces at die interfaces, determine the metallurgical interactions occurring at the interfaces with the dies, and investigate the consequences of extreme temperatures on material flow, microstructural evolution, and resultant properties.

Summary

Solid Phase Processing of high flow stress materials, particularly within the critical classes of structural and functional materials, often requires high temperature and force. Operating under such extreme processing conditions presents challenges related to tool/die survival as well as efficient management of process energy. The goal of this project is to explore the underpinning science of these challenges; how materials respond to high shear at die interfaces, what the metallurgical contact conditions with the dies, and how the extreme temperature affects material flow, microstructure, and properties during ShAPE, friction extrusions, and other allied processes. In our prior research, we have observed notable damage, distortion, and wear on tools and dies when processing temperatures exceed 800°C. For Solid Phase Processing (SPP) to emerge as a viable and advanced manufacturing platform, it is imperative that we elucidate the interaction between the dies and the processed materials. This understanding is pivotal not only for demonstrating extraordinary material properties but also for achieving reliability and scalability in the manufacturing process.

In previous SPP research, it has been observed that the interactions between tooling components and billets are dependent on the composition of the tools and billet material and details of the processing parameters used. In certain instances, billet material sticks to the dies, while in others, the dies remain clean after extrusion. The occurrence of sticking, particularly at elevated temperatures or, in some cases, at high extrusion speeds, suggests the existence of a "dead metal" zone near the die. This zone may exhibit distinct levels of strain or heat generation compared to the adjacent material undergoing plasticization. These observations have far-reaching implications for fundamental aspects such as flow dynamics, temperature profiles, advection, strain, and strain rate. A more profound understanding of die/billet or tool/workpiece interactions under extreme processing conditions would serve several critical purposes: (1) enhances our understanding of the deformation state and thermomechanical history of the materials, (2) enable us to make more informed predictions and select optimal process variables that can facilitate the creation of desired microstructures while preserving the longevity of dies, particularly as we transition to extreme processing conditions and ((3) provides essential data for the calibration and validation of the predictive capabilities of the SPH (Smoothed Particle Hydrodynamics) process models currently under development in Thrust 1 Project 3. This research also extends our computational modeling capabilities to encompass extreme thermomechanical conditions.

Acknowledgments

This research was supported by the Solid Phase Processing Science Initiative, under the Laboratory Directed Research and Development (LDRD) Program at Pacific Northwest National Laboratory (PNNL). PNNL is a multi-program national laboratory operated for the U.S. Department of Energy (DOE) by Battelle Memorial Institute under Contract No. DE-AC05-76RL01830.

Acronyms and Abbreviations

SPH: Smoothed Particle Hydrodynamics
HT: Heat Treated
ShAPE: Shear Assisted Processing and Extrusion
XPS: X-ray Photoelectron Spectroscopy
OM: Optical Microscopy
SEM: Scanning Electron Microscopy
XCT: X-ray Computed Tomography

Contents

Abstract ii
Summary iii
Acknowledgments iv
Acronyms and Abbreviations v
1.0 Introduction 1
2.0 Materials and Experimental Methods 3
2.1 Die-Billet Contact Condition 3
2.2 Indirect vs. Direct Friction Extrusion 4
3.0 Results and Discussions 5
3.1 Development of Sticking and Non-sticking Conditions 5
3.2 Smoothed Particle Hydrodynamic (SPH) Model to Understand Contact Condition 8
3.3 Indirect and Direct Friction Extrusions 11
4.0 Conclusions 13
5.0 References 14

Figures

Figure 1: Scrolled die faces before friction extrusion process: (a) MP159 after heat treatment and then machined, (b) MP159 after machine and then heat treatment, and (c) W-Re die. 3
Figure 2: (a) Indirect friction extrusion process, (b) direct friction extrusion process, (c) tooling for direct extrusion, (d) die and stationary can assembly for direct extrusion, (e-f) secondary ram set up in ShAPE machine for direct extrusion. 4
Figure 3: Different die surfaces before and after friction extrusion: (a) MP159 die heat treated and then machined and extruded below 750ºC, (b) MP159 die heat treated and then machined and extruded above 750ºC, (c) MP159 die machined and then heat treated and extruded above 750ºC, (d) W-Re die extruded at any process temperature (low to high) 5
Figure 4: High energy resolution narrow scan X-ray photoelectron spectra of selected elemental regions: (a) Ni, (b) Co, (c) Cr, (d) Mo, (e) Ti, and (f) Al 6
Figure 5: (a) Optical microscopic image of die-billet remnant cross sections through the center of the extruded Cu wire, (b) low- and (c) medium-resolution SEM images at the flat surface of the MP159 die. 7
Figure 6: (a) High resolution SEM image of the Cu-MP159 die interface, (b) elemental mapping for Cr and O to detect the darker oxide later at the imterface, and (c) EDS mapping at the interface for O, Ti, Al and Cr. 7
Figure 7: (a) SPH model set up to simulate the experimental condition during friction extrusion (b) friction extrusion scroll die model. 8

Figure 8: (a) Effective plastic strain and (b) temperature field for slipping condition, (c) Effective plastic strain and (d) temperature field for sticking condition from SPH simulation, (e) billet remnant from experimental evidence showing higher plastic deformation near the center at two scrolled region and lower deformation near the edge with smooth surface in slipping condition, (f) billet remnant from experimental evidence showing higher plastic deformation at the edge (rough surface) that appeared not to contribute to the spontaneous extrusion, (g) central part of billet remnant stuck with die face.....9

Figure 9: SPH model-predicted contour plots of (a) Strain rate- (b) Circumferential velocity- (c) Radial velocity- (d) Longitudinal velocity in slipping conditions and (a) Strain rate- (b) Circumferential velocity- (c) Radial velocity- (d) Longitudinal velocity in sticking conditions. 10

Figure 10: Material flow analyses with using marker material: SPH model-predicted results for - (a) slipping and (b) sticking condition, and experimental evinces from XCT scan of Cu wire with marker for- (c) slipping and (d) sticking condition.....10

Figure 11: Comparison of average plastic strain in wire for slipping and sticking conditions.....11

Figure 12: (a) Friction extrusion aluminum wire, 300 mm long, (b) Die and flash after direct extrusion, (c) Die and flash after indirect extrusion, (d)-(f) Torque, die face temperature, and tailstock force of direct and indirect extrusion.....12

1.0 Introduction

Numerous materials critical for enhancing the security and resilience of the US energy infrastructure, such as steels, nickel alloys, and metal composites, demand synthesis and manufacturing processes conducted under conditions of extreme temperature and pressure. The processing of these materials using solid-phase processing methods necessitates exceptionally durable tool and die materials, along with a paradigm shift in how we handle the generation of extreme heat.

The previous research has had a significant impact on our understanding of the thermomechanical history imposed during friction extrusion of cylindrical wires [1-3]. In a nutshell, these works involved measuring three orthogonal plastic strain components across a wide range of extrusion parameters through the use of inserted markers. Several salient points were elucidated by the work done. First and foremost, it was observed that the level of imposed strain was primarily influenced by the ratio of the extrusion die's advance rate to its rotation rate, commonly referred to as the die advance per revolution (DAPR). Secondly, the presence of strain transients at the beginning of extrusions pointed to the formation of a dead metal zone. Thirdly, when comparing strains observed using flat and scrolled dies, it was noted that in many cases, though not all, there was no significant difference. All three of these observations collectively suggest that the primary contact condition between the die and the workpiece is either fully sticking or very close to it. This conclusion was further corroborated by the results of a high-fidelity simulation using smoothed particle hydrodynamics (SPH). The SPH simulation of the process demonstrated that full sticking conditions closely matched the strains measured experimentally [4].

Variability in sticking behavior between workpiece and tool materials has been observed in friction stir welding (FSW). In research conducted at the University of South Carolina for the Center for Friction Stir Processing, an interesting observation was made during FSW of Ti-6Al-4V: the weld materials adhere to W-Re alloy tools but not to W-La_2O_3 tools. This sticking phenomenon becomes more prevalent with higher levels of Re in the tool alloy and for weld conducted at higher temperatures. Consultation with Rhenium Alloys, the producer of tool material, suggested that the titanium strongly reacts with the rhenium in the alloys resulting in the observed sticking behavior [5]. Furthermore, in the case of FSW of steel, it was noticed that polycrystalline cubic boron nitride (PCBN) tools exhibited lower torques and power inputs compared to similar tungsten tools. These findings highlight the significant impact that interactions between tool materials and workpieces, or in the case of friction extrusion, die materials, and billets can have on process response variables. Consequently, these interactions can influence the microstructure and properties of the extrudate.

While there is a substantial body of research on Tribology, it has traditionally focused on various aspects of friction, wear, and lubrication, particularly under different temperature conditions. However, there is indeed a gap in the literature when it comes to understanding how tool/workpiece interactions specifically impact bulk deformation in the workpiece, especially in the context of friction extrusion. Conventional extrusion processes typically aim to minimize friction on the die face using lubricants, which can reduce wear and facilitate smoother extrusions. In contrast, in processes like friction extrusion and shear assisted processing and extrusions (ShAPE), there may be a deliberate interest in enhancing friction between the tool and workpiece to achieve specific material properties or deformation characteristics.

This unique aspect of ShAPE and similar processes presents an exciting opportunity for further research and exploration. Investigating how controlled tool/workpiece interactions can influence

the outcome of extrusion processes, such as microstructure, mechanical properties, and overall material behavior, can provide valuable insights and potentially lead to innovations in advanced manufacturing techniques. It's an area where interdisciplinary research combining materials science, tribology, and process engineering can make significant contributions.

In this study, our aim is to conduct experimental assessments that encompass two contrasting die/billet interactions: one characterized as "slippery" (non-sticking) and the other as "sticky." The primary objective is to investigate how these differing contact conditions influence the essential process parameters required to achieve metallurgically and mechanically sound extrusions. The dataset generated through these experimental conditions will be subsequently integrated into a mesh-free SPH process model. This will assist in determining how the model should handle various contact conditions. Following this, calibration and validation of the model will be carried out to ensure its accuracy and reliability. Furthermore, the insights gained from the tasks will be extended to a comparative analysis of direct and indirect friction extrusion processing conditions. Notably, this study represents a pioneering effort as it explores the novel concept of direct friction extrusion, where the die does not plunge into the billet within the container. Instead, the billet is fed using a secondary ram, resulting in the production of direct extrusions, wherein both the ram and extrusion occur in the same direction.

2.0 Materials and Experimental Methods

2.1 Die-Billet Contact Condition

The C10100 precursors were inserted with Cu-Graphite composite wire markers to investigate material flow. This marker insertion technique was adopted from previous studies [1, 2, 6]. It's important to note that the Cu-Gr markers were also produced using the friction extrusion process described in [7]. All tooling dimensions and materials preparation for an extrusion ratio of 100:1 were adopted from earlier research, and thus, they won't be reiterated here for the sake of brevity [1,2].

However, to assess the impact of different contact conditions on process parameters, two types of die materials were chosen for producing metallurgically and mechanically sound Cu wire extrusions: (1) Ni-Co-Cr based alloy, MP159, and (2) W-Re. MP159 was selected in two conditions: (a) heat treated (HT) followed by machining and (b) machining followed by heat treatment. The heat treatment of MP159 dies was carried out at 660°C for 4 hours in an inert (argon) atmosphere, followed by quenching in the laboratory environment. All the extrusions were performed using a one-of-its-kind Shear Assisted Processing and Extrusion (ShAPE) machine at PNNL.

Based on previous research on the same material and after conducting several experimental trials, a specific set of friction extrusion parameters was selected, which included a rotational speed of 85 RPM, a feed rate of 4 mm/min, and an experimental cutoff temperature of 750°C. These parameters were used for three extrusions, employing three different dies: (a) MP159-HT followed by machining, (b) MP159-machined followed by HT, and (c) W-Re die. Figure 1 displays the surfaces of the MP159 and W-Re tools prior to the friction extrusion process.

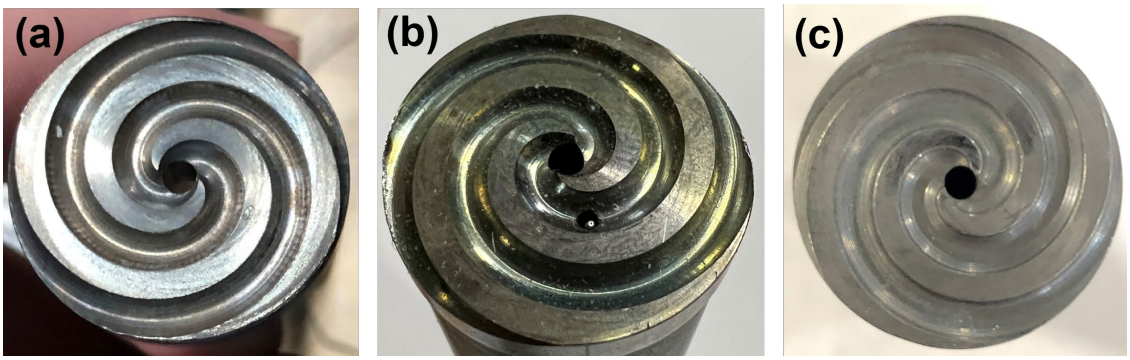

Figure 1: Scrolled die faces before friction extrusion process: (a) MP159 after heat treatment and then machined, (b) MP159 after machine and then heat treatment, and (c) W-Re die.

The die surface chemistry of MP159 in conditions (a) and (b), as previously mentioned, was assessed using X-ray photoelectron spectroscopy. To examine the cross-section of the die-billet remnant in the sticking condition, optical microscopy (OM) and scanning electron microscopy (SEM) was employed. Furthermore, the extruded Cu wire underwent characterization utilizing optical microscopy and 3D X-ray computed tomography (XCT) techniques.

2.2 Indirect vs. Direct Friction Extrusion

Up until now, all friction extrusion experiments documented in the literature have been conducted using the indirect or back extrusion method. In this method, the die plunges into the billet, resulting in the ram direction and extrusion direction being opposite, as illustrated in Figure 2-a. This process necessitates the die's interaction with the billet container, and under extreme processing conditions, it often leads to galling with the liner/can at high temperatures, causing the die to weld to the container.

Hence, this marks the first instance where we present modifications to the tools and manufacturing processes for carrying out direct friction extrusion. In this scenario, the rotating die is positioned only at the opening of the container, and the billet is pushed into the die using the ram, as depicted in Figure 2-b. Consequently, the interaction between the die and liner was eliminated.

Figures 2(c-f) showcase the tooling and setup required for executing direct extrusion in the ShAPE machine. To demonstrate and compare the outcomes between indirect and direct extrusions, we applied a rotational speed of 300 RPM and a ram speed of 8 mm/min using flat dies. These settings were employed to extrude a 4.5 mm diameter Al wire (AA1100 with an AA20250 marker, like in [2]), however maintaining an extrusion ratio of 32:1.

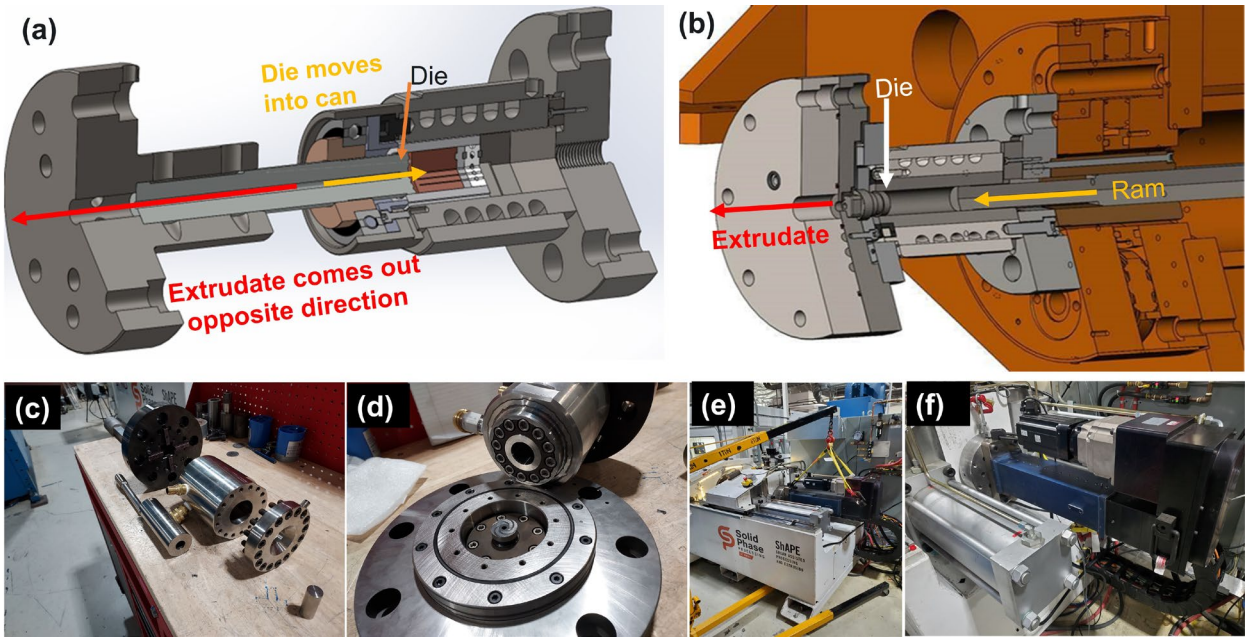

Figure 2: (a) Indirect friction extrusion process, (b) direct friction extrusion process, (c) tooling for direct extrusion, (d) die and stationary can assembly for direct extrusion, (e-f) secondary ram set up in ShAPE machine for direct extrusion.

3.0 Results and Discussions

3.1 Development of Sticking and Non-sticking Conditions

Figure 3 illustrates the contrasting appearances of the die surfaces before and after the extrusion of Cu wires. When the MP159 tool blank undergoes heat treatment and is subsequently machined to achieve the desired die shape and features (scrolls), there is no evidence of sticking during Cu extrusion below 750°C, as depicted in Figure 3-a. However, when the same die is operated above 750°C, as shown in Figure 3-b, sticking conditions arise, indicating an interfacial reaction between the die and billet at elevated temperatures. In contrast, when the heat treatment of the MP159 die is conducted after the machining process and the incorporation of geometric features, Cu is not sticking even at elevated temperatures above 750°C, as demonstrated in Figure 3-c. This suggests that specific tool surface conditions created during the heat treatment prevent sticking, even under higher-temperature conditions. Interestingly, the W-Re tool exhibits a non-sticking behavior with Cu at any temperature and under various extrusion conditions, as observed in Figure 3-d.

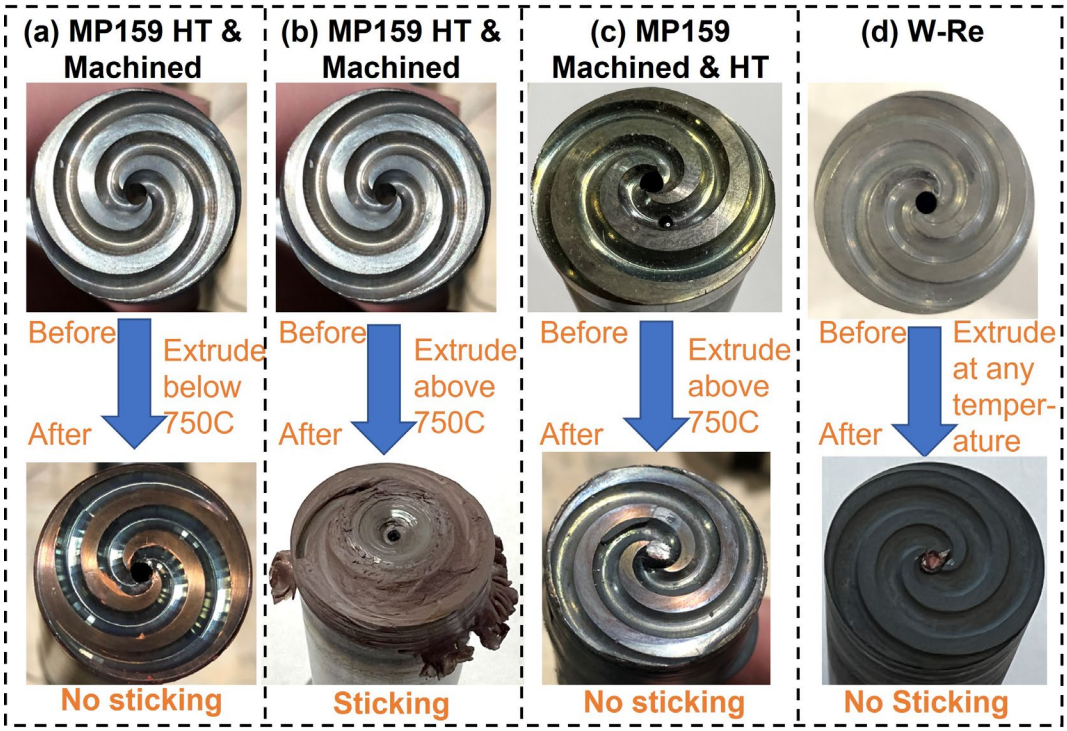

Figure 3: Different die surfaces before and after friction extrusion: (a) MP159 die heat treated and then machined and extruded below 750ºC, (b) MP159 die heat treated and then machined and extruded above 750ºC, (c) MP159 die machined and then heat treated and extruded above 750ºC, (d) W-Re die extruded at any process temperature (low to high)

To analyze the elemental composition, surface chemistry, and oxidation state of the two conditions within the MP159 die, XPS characterization was conducted. The initial, shiny state of the heat-treated and machined MP159 surface, as depicted in Figure 1-a, is referred to as HT + M. Conversely, the oxidized, greenish condition of the machined and subsequently heat-treated surface is denoted as M + HT in the subsequent XPS analyses. It's important to note that XPS

is highly sensitive to the chemical states of surface elements and contaminants, providing insights into the surface within a depth range of 1-10 nm. As a result, this study focuses on selected alloying elements within MP159, namely Ni, Co, Cr, Mo, Ti, and Al. Figure 4 (a-f) showcases high-resolution narrow scan spectra for these key alloying elements of MP159. Across all the XPS spectra, there is evidence of a reduction in metallic bonding on the surface that underwent heat treatment after machining (M + HT), in comparison to the freshly machined surface (HT + M). Furthermore, the presence of Ni, Co, and Cr oxide peaks is more pronounced on the M + HT surface. Moreover, the observed shifts in the spectral peaks, noted in the element's binding energy at 854.3 eV, 796.5 eV, 576.7 eV, 229.6 eV, 458.7 eV, and 74.5 eV, respectively, indicate the corresponding formation of metal oxides: NiO, CoO, Cr_2O_3, MoO_2, TiO_2, and Al_2O_3 [8].

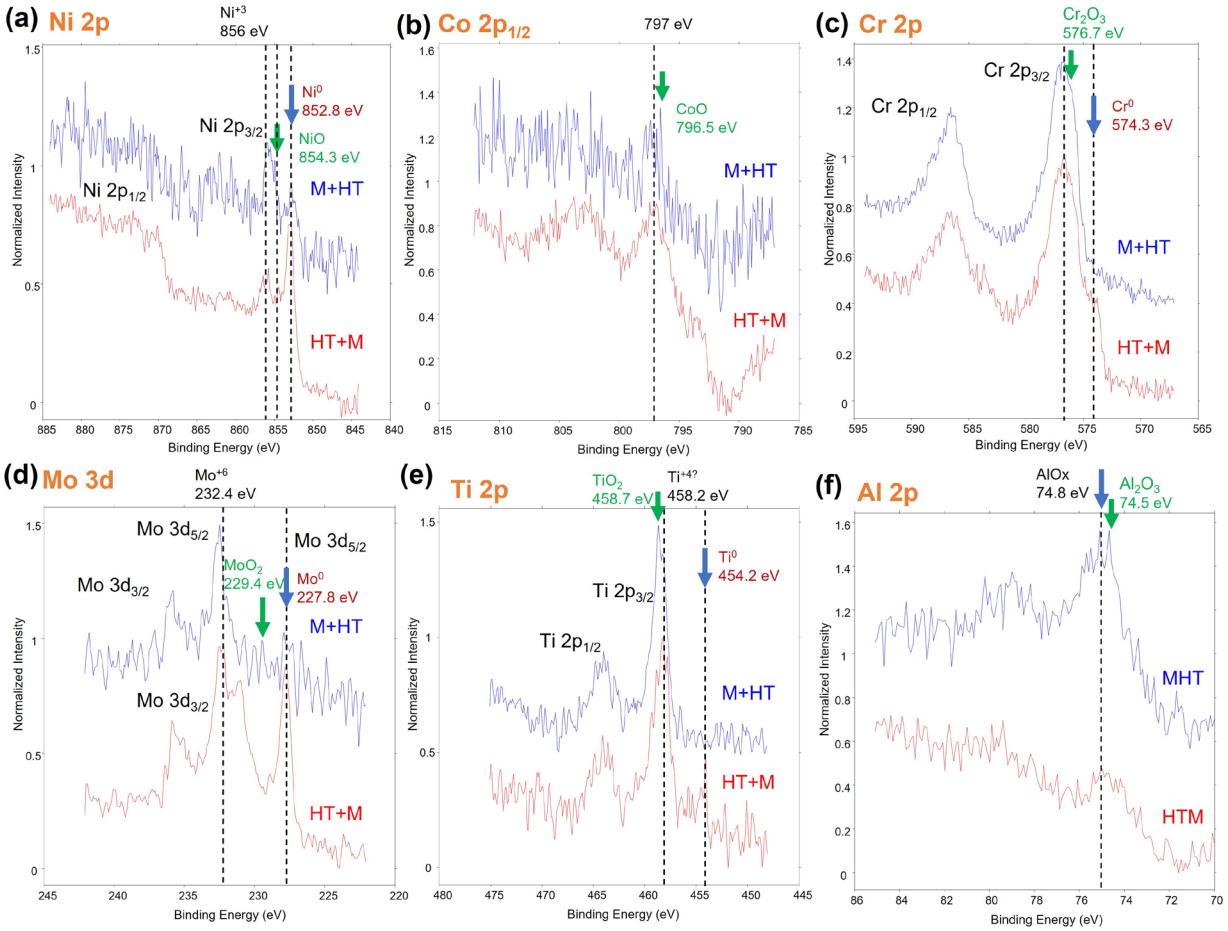

Figure 4: High energy resolution narrow scan X-ray photoelectron spectra of selected elemental regions: (a) Ni, (b) Co, (c) Cr, (d) Mo, (e) Ti, and (f) Al

The sticking MP159-Cu interface shown in Figure 3-b was further investigated under the SEM to understand the interfacial bonding state between the MP159 die and Cu billet remnant. Figure 5-a depicts the OM image of the cross-section of the die-billet remnant bonded part along with the friction-extruded Cu wire at the center. The low and medium-resolution SEM micrographs in Figures 5 b and c revealed no obvious interfacial reaction at these scales, but good intimate bonding with recrystallized grains on the boundary. However, high-resolution SEM images with EDS mapping of chemical composition in Figure 6 (a-c) revealed the presence of discontinuous,

agglomerated oxide particles at the tool die-billet remnant interfaces but mostly the contact interface was intimately bonded in the case of heat-treated and then machined MP159 dies. However, machined and then heat-treated MP159 die surfaces prevent this bonding because of the abundance of these oxide layers.

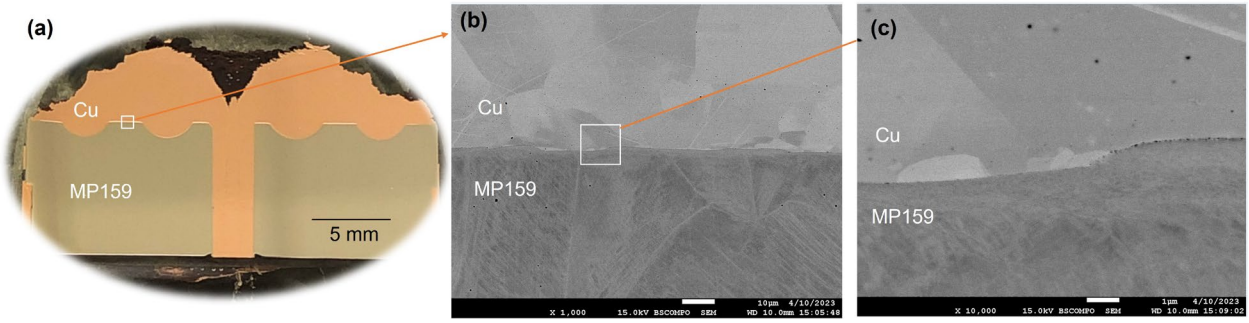

Figure 5: (a) Optical microscopic image of die-billet remnant cross sections through the center of the extruded Cu wire, (b) low- and (c) medium-resolution SEM images at the flat surface of the MP159 die.

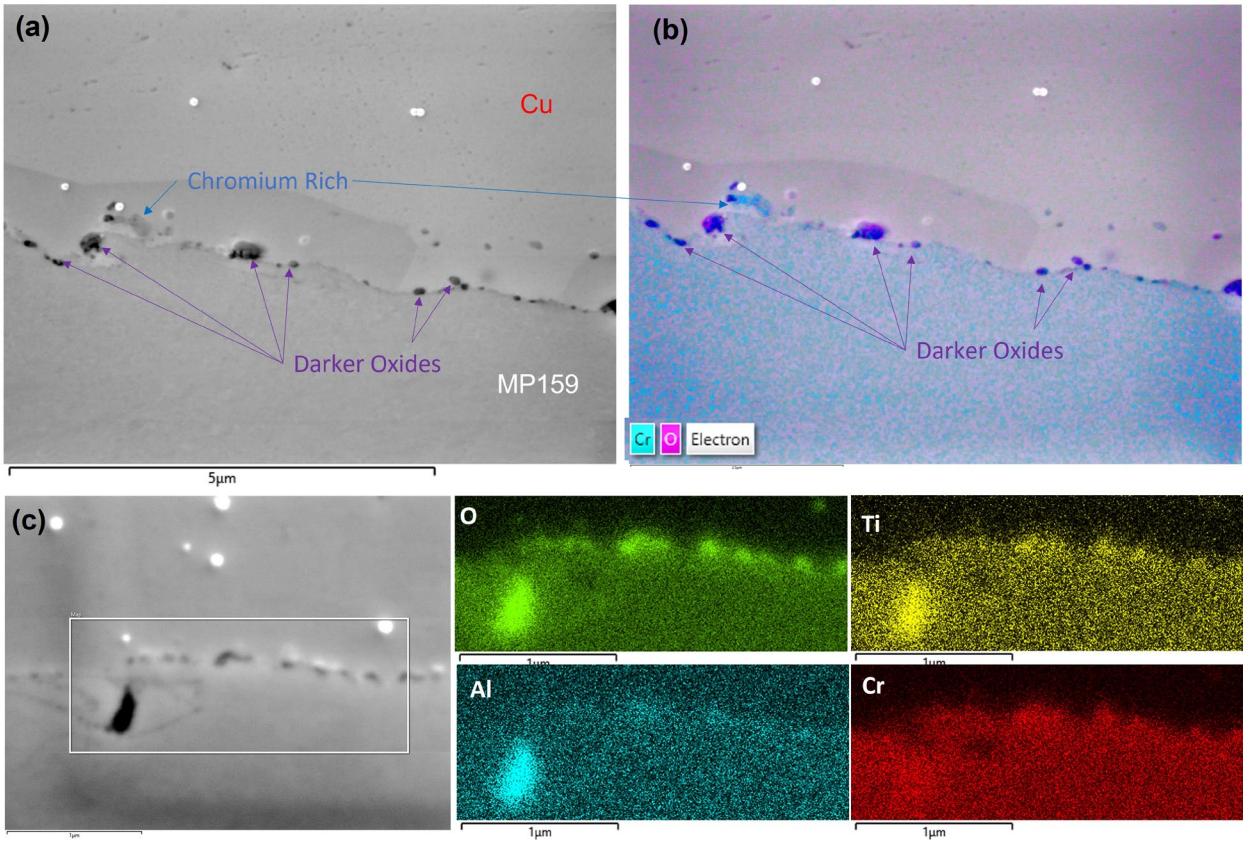

Figure 6: (a) High resolution SEM image of the Cu-MP159 die interface, (b) elemental mapping for Cr and O to detect the darker oxide later at the imterface, and (c) EDS mapping at the interface for O, Ti, Al and Cr.

3.2 Smoothed Particle Hydrodynamic (SPH) Model to Understand Contact Condition

SPH is a mesh-free computational frameworks developed for the friction extrusion process under the SPPSi Thrust 1 Project 3. Several journal articles were published [4, 9] in which model descriptions and methods are elaborated therefore are not repeated in this report. Figure 7 (a-b) illustrates the SPH model setup to replicate the experimental boundary conditions and process parameter configurations (rotational speed of 85 RPM and ram speed of 4 mm/min). For the thermomechanical properties of Cu, the Johnson-Cook model was utilized, and the contact between the tool and billet was defined using the Coulomb-Tresca law. To account for the thermal boundary conditions during the cooling of the billet container, ghosted SPH particles were used in the inner container and die face. Sticking and slipping contact conditions were achieved by specifying distinct friction parameters (μ_f), where larger μ_f values promote sticking behavior, while a small μ_f value of 0.2 makes slipping more likely to occur.

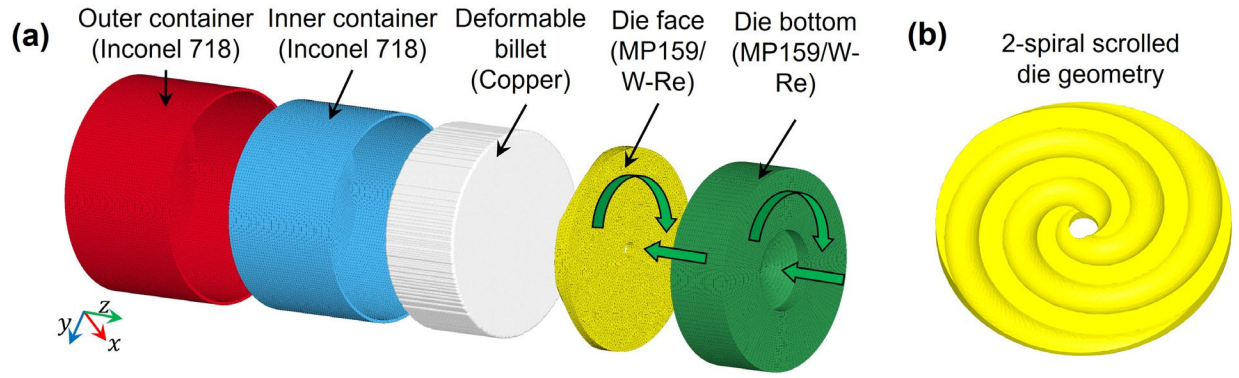

Figure 7: (a) SPH model set up to simulate the experimental condition during friction extrusion (b) friction extrusion scroll die model.

Figure 8 (a-d) displays the model-predicted central cross-sectional effective plastic strain and temperature fields for both slipping and sticking conditions. In Figure 8 (a-b), we observe lower levels of plastic deformation and temperature near the billet corner in the case of slipping. Here, plastic strain and temperature are notably higher near the extrusion hole where the sharp scrolls are situated within the die. This low strain on the edges in the SPH model aligns with the experimental findings, as demonstrated in Figure 8 (e), where only billet material near the extrusion hole flows within the die groove during the retraction phase. Conversely, under sticking conditions, as shown in Figure 8 (c), plastic strain is much higher at the billet corner, where the material rotates with the die and does not extrude. This creates the impression of a dead metal zone scenario during friction extrusion. However, the temperature generated is more uniformly distributed along the billet interface, as seen in Figure 8 (d). The shape of the high-plasticity zone also corresponds with the experimental results. Figure 8 (f) reveals a highly deformed zone at the periphery of the billet remnant, while the billet center remains stuck to the die, as depicted in Figure 8 (g).

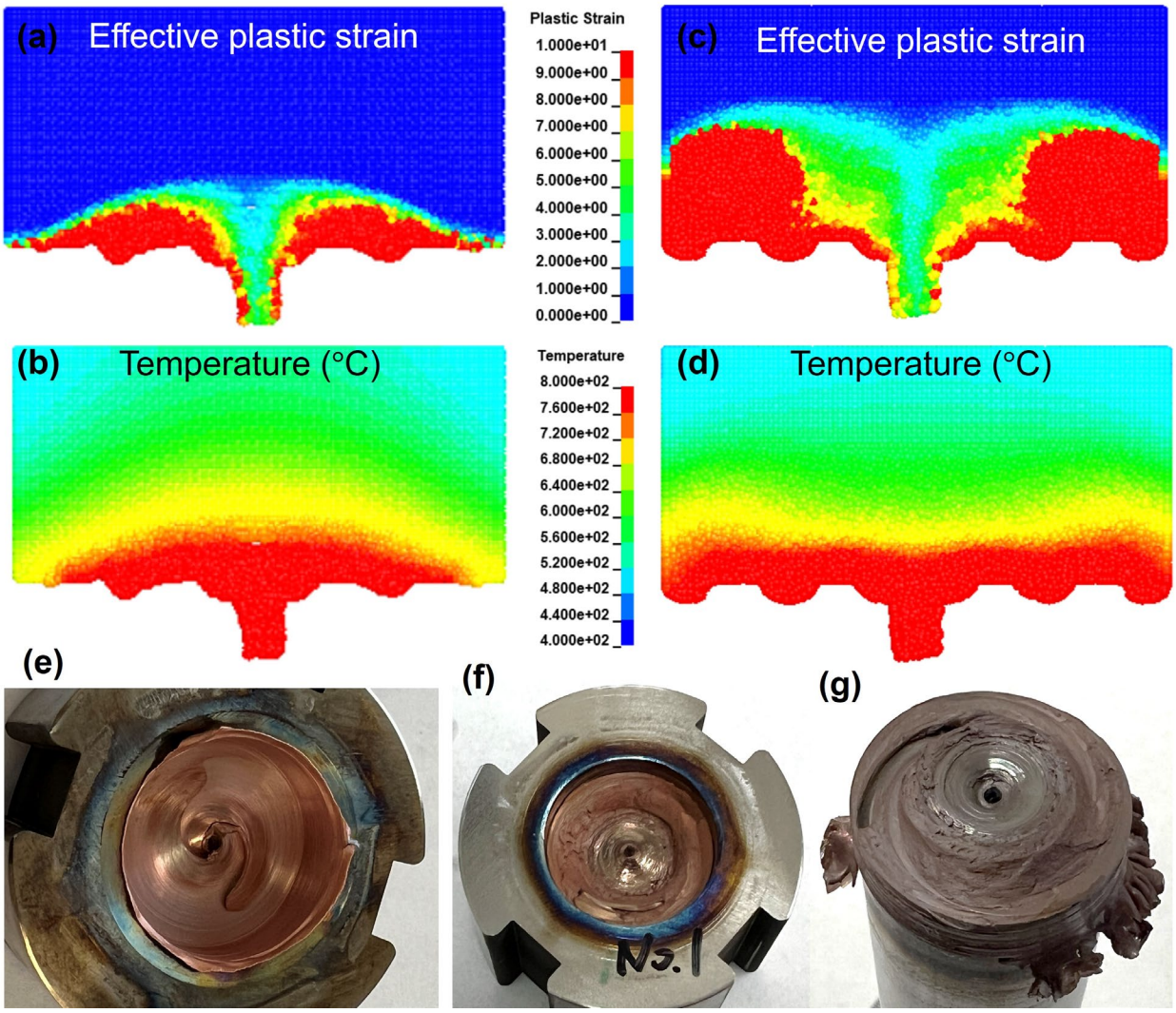

Figure 8: (a) Effective plastic strain and (b) temperature field for slipping condition, (c) Effective plastic strain and (d) temperature field for sticking condition from SPH simulation, (e) billet remnant from experimental evidence showing higher plastic deformation near the center at two scrolled region and lower deformation near the edge with smooth surface in slipping condition, (f) billet remnant from experimental evidence showing higher plastic deformation at the edge (rough surface) that appeared not to contribute to the spontaneous extrusion, (g) central part of billet remnant stuck with die face.

Figure 9 displays contour plots illustrating the strain rate and material velocity for both slipping (Figure 9 a-d) and sticking (Figure 9 e-h) conditions. In Figure 9-a, we observe a high strain rate in slipping conditions, primarily due to the relative motion occurring at the billet/die interface. Conversely, the strain rate along the billet/die interface is notably smaller in sticking conditions (Figure 9-e) because the billet material adheres and moves in unison with the die at a high speed. Consequently, the X-velocity also becomes higher in sticking conditions (Figure 9-f) compared to slipping conditions (Figure 9-b). As a result of the sticking phenomenon, the billet materials above the contact surface undergo more deformation. Notably, the region with a high X-velocity in the sticking case corresponds to a low Z-velocity (as depicted in Figure 9-h), indicating that materials are rotating rather than being extruded.

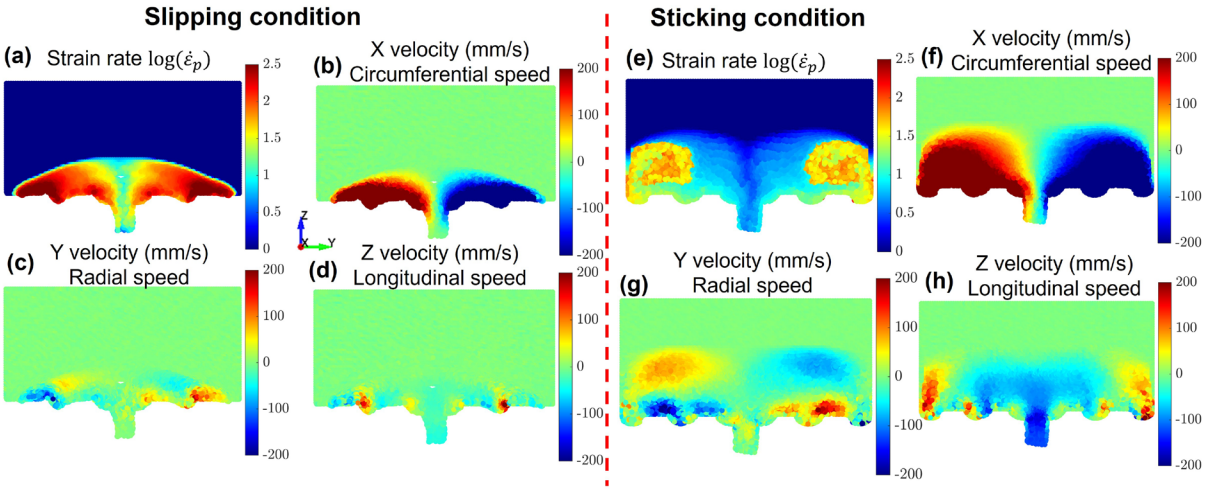

Figure 9: SPH model-predicted contour plots of (a) Strain rate- (b) Circumferential velocity- (c) Radial velocity- (d) Longitudinal velocity in slipping conditions and (a) Strain rate- (b) Circumferential velocity- (c) Radial velocity- (d) Longitudinal velocity in sticking conditions.

In line with the marker material tracing used in the experimental method, the SPH approach was also employed to analyze material flow patterns using a marker tracer. Figure 10 presents a comparison between the SPH marker tracing and XCT scans of the marker material from experimental data. Remarkably, the SPH model consistently predicts the material flow in both sticking and slipping conditions. In the sticking condition (Figure 10-b), the marker material within the billet rotates with the die several times before eventually being extruded out. Conversely, in the slipping condition (Figure 10-a), the marker material flow is disrupted at the die/billet interface, leading to a distinct material behavior.

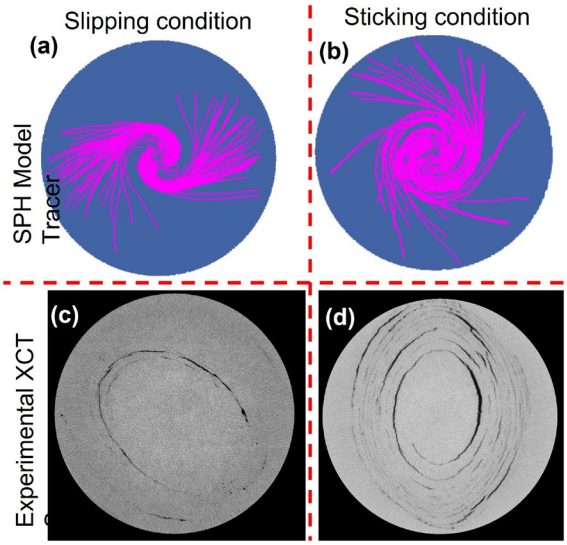

Figure 10: Material flow analyses with using marker material: SPH model-predicted results for - (a) slipping and (b) sticking condition, and experimental evinces from XCT scan of Cu wire with marker for- (c) slipping and (d) sticking condition.

Figure 11 presents the plastic strain analyses on the wire for slipping and sticking conditions. From the contour plot of plastic strain and the graph, it was evident that the wire materials experienced 71.8% more plastic strain in the sticking condition (ε= 12.2) than the strain in the slipping condition (ε=7.1). This is important evidence since more strain could be important for systems that need more mixing, for example in the extrusion scenario of metal matrix composites (MMC) or highly nonhomogeneous feedstock.

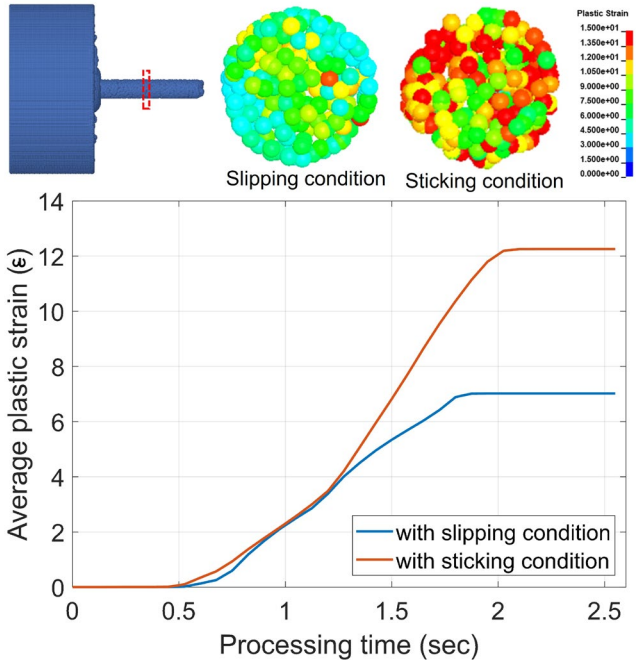

Figure 11: Comparison of average plastic strain in wire for slipping and sticking conditions.

3.3 Indirect and Direct Friction Extrusions

4.5 mm diameter Aluminum wire was extruded in both indirect and direct extrusion modes, shown in Figure 12 (a). After extrusion, the flat dies were inspected, and the “flash” conditions are presented in Figure 12 (b) and (c). Direct extrusion generated a very short flash and indirect extrusion produced flash around the die cylindrical surface (flash thickness about 0.4 mm and length 25 mm) as it plunged into the billet. This is as expected since the die was inserted deep into the ring in the indirect extrusion mode. One of the benefits of direct extrusion is minimizing flash production which yields a higher volume of extrusions (minimizing waste). Also, less flash reduces the frictional force between the die and the ring, thus reducing the torque, power, and force required in friction extrusion.

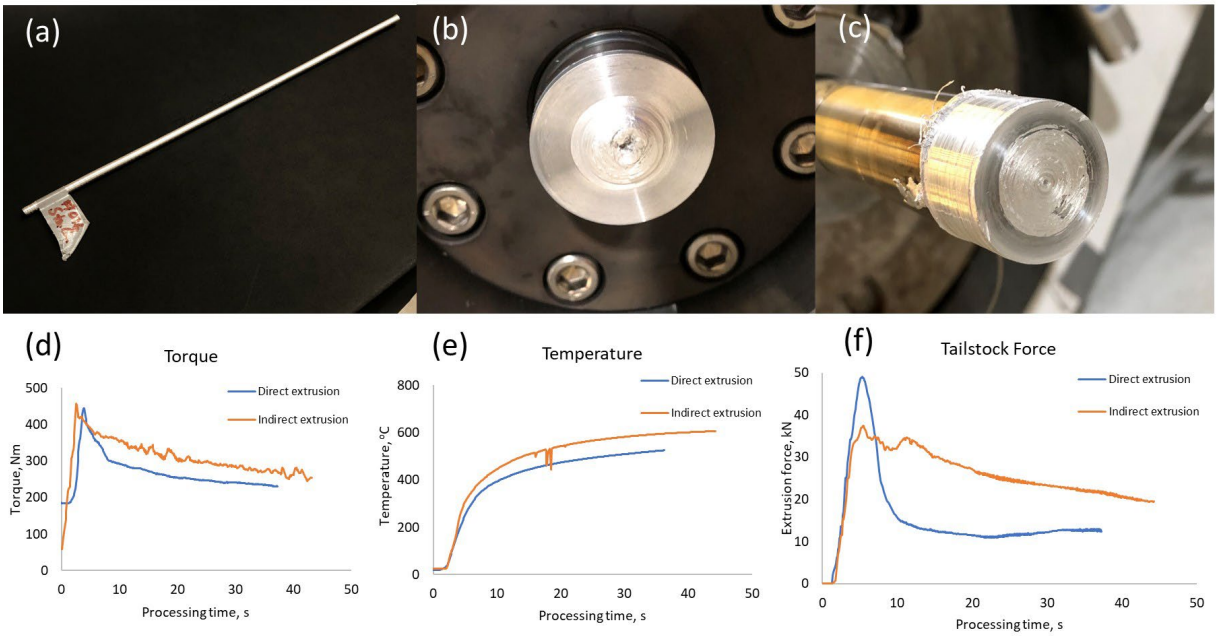

Figure 12: (a) Friction extrusion aluminum wire, 300 mm long, (b) Die and flash after direct extrusion, (c) Die and flash after indirect extrusion, (d)-(f) Torque, die face temperature, and tailstock force of direct and indirect extrusion.

Figure 12 (d) compares the extrusion torque between direct and indirect extrusion. Although breakthrough torques at the beginning of extrusion are almost identical for direct and indirect extrusions, direct extrusion has 10% less steady-state torque than indirect extrusion, indicating that the power of direct extrusion is also 10% less. Comparing the die temperature shown in Figure 12 (e), direct extrusion has a lower processing temperature compared to indirect extrusion. We believe there are two reasons: (1) different machine setup has different thermal boundary conditions, which led to different heat transfer rates, or, (2) indirect extrusion has more frictional heat caused by die-flash-ring interaction. Figure 12(f) illustrates the direct and indirect extrusion forces, both monitored using a load cell on the container mounting plate. In the case of indirect extrusion, the measured force corresponds to the extrusion force. Conversely, in direct extrusion, the extrusion force combines the ram force with the load cell measurement. Remarkably, the initial breakthrough (peak) force for direct extrusion (48 kN) exceeded that of indirect extrusion (38 kN) by approximately 26%. However, direct extrusion swiftly stabilizes after surpassing the breakthrough force, maintaining a consistent extrusion force of approximately 12 kN. This steady extrusion force for direct extrusion is at least 50% lower than the extrusion force observed in the latter stages of indirect extrusion. Notably, even with extended processing time, indirect extrusion fails to exhibit a steady force response.

4.0 Conclusions

This project has significantly advanced the understanding of extreme solid phase processing conditions through the introduction of robust tools (made of MP159, W-Re) and equipment (secondary ram with stationary can assembly for direct extrusion). The knowledge developed through this project enables the development of a synergistic SPH model and experimental validation for friction extrusion. Notably, we've identified key factors influencing die-workpiece contact conditions, such as the surprising effectiveness of a thin oxide layer on MP159 dies to prevent sticking even at elevated temperatures. This discovery allows for controlled adjustment of contact conditions by modifying specific parameters. Consequently, tool material requirements can be optimized, and die-coating chemistry can be tailored to enhance or reduce sticking. The lessons learned will be applied in programmatic work involving ODS steel, stainless steel, Ti, Cu, Zr alloys, and their metal matrix composites. However, the path ahead involves further research to incorporate essential physical properties of tool materials, such as thermal conductivity, heat capacity, and surface roughness, into the SPH model and experimental validation, with a particular focus on analyzing slip-stick conditions in friction extrusion. Additionally, enhancing the model requires the development of a physics-informed friction coefficient based on the billet-die thermomechanical conditions.

5.0 References

1. Li, X., M. Reza-E-Rabby, A. Guzman, G. Grant, S. Mathaudhu, M. Hinton, A. Reynolds, Strain and strain rate in friction extrusion, Journal of Materials Research and Technology 20 (2022) 882-893.

2. Li, S., M. Reza-E-Rabby, M. Ryan, G. Grant, A. Reynolds, Evaluation of orthogonal strain components in friction extrusion, Journal of Materials Research and Technology 15 (2021) 3357-3364.

3. Reza-E-Rabby, M., X. Li, G. Grant, S. Mathaudhu, A. Reynolds, Process parameters and system responses in friction extrusion, Journal of Manufacturing Processes 85 (2023) 21-30.

4. Li, L., V. Gupta, X. Li, A.P. Reynolds, G. Grant, A. Soulami, Meshfree simulation and experimental validation of extreme thermomechanical conditions in friction stir extrusion, Computational Particle Mechanics 1-21.

5. Leonhardt, T., FSW of Ti alloys using W based tool from Rhenium Alloys, in: G.G. Anthony P. Reynolds (Ed.) 2015.

6. Li, X., W. Tang, A. Reynolds, W. Tayon, C. Brice, Strain and texture in friction extrusion of aluminum wire, Journal of Materials Processing Technology 229 (2016) 191-198.

7. Li, X., C. Zhou, N. Overman, X. Ma, N. Canfield, K. Kappagantula, J. Schroth, G. Grant, Copper carbon composite wire with a uniform carbon dispersion made by friction extrusion, Journal of Manufacturing Processes 65 (2021) 397-406.

8. National Institute of Standards and Technology, NIST X-ray Photoelectron Spectroscopy Database, NIST Standard Reference Database Number 20, Version 4.1, 2000.

9. Li, L., M. Reza-E-Rabby, N. Overman, T. Wang, S. Whalen, G. Grant, S. Mathaudhu, A. Soulami, Analysis of contact conditions and microstructure evolution in shear assisted processing and extrusion using smoothed particle hydrodynamics method, Materials & Design 221 (2022) 111010.

Pacific Northwest National Laboratory

902 Battelle Boulevard
P.O. Box 999
Richland, WA 99354

1-888-375-PNNL (7665)

www.pnnl.gov